ACSNANO

www.acsnano.org

ARTICLE

Laser-Driven Growth of Semiconductor Nanowires from Colloidal Nanocrystals

Elena P. Pandres,[#] Matthew J. Crane,[#] E. James Davis, Peter J. Pauzauskie,[*] and Vincent C. Holmberg[*]

Cite This: https://doi.org/10.1021/acsnano.1c00683

Read Online

ACCESS | Metrics & More | Article Recommendations | Supporting Information

ABSTRACT: Semiconductor nanowire production through vapor- and solution-based processes has propelled nanowire systems toward a wide range of technological applications. Although vapor-based nanowire syntheses enable precise control over nanowire composition and phase, they typically employ batch processes with specialized pressure management systems, limiting throughput. Solution-based nanowire growth processes have improved scalability but can require even more extensive pressure and temperature management systems. Here, we demonstrate a solution-based nanowire growth process that utilizes the large Young−Laplace interfacial surface pressures and collective heating effects of colloidal metal nanocrystals under irradiation to drive nanowire growth photothermally. Laser irradiation of a solution containing metal nanocrystals and semiconductor precursors facilitates rapid heating, precursor decomposition, and nanowire growth on a benchtop in simple glassware under standard conditions, potentially enabling a range of solution-based experiments including in-line combinatorial identification of optimized reaction parameters, *in situ* measurements, and the production of nanowires with complex compositions.

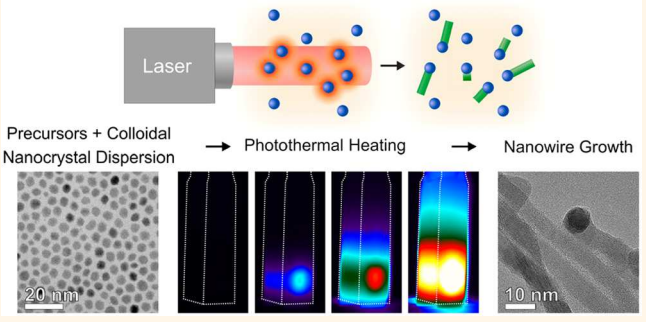

KEYWORDS: *solution-liquid-solid, nanowire, semiconductor, nanocrystal, photothermal, Young−Laplace, heat transfer*

Light absorption can be used as a handle to initiate chemical reactions in a wide range of materials, enabling key processes for diverse applications. For example, light absorption by photosensitive molecules has been used to engineer advanced biomaterials[1,2] as well as to initiate surface reactions, which impart additional functionality to inorganic materials.[3,4] Inorganic nanomaterials can also participate in light-driven energy transfer processes to drive chemical reactions[5−12] and phase transformations.[13−17] For instance, the solar irradiation of plasmonic colloidal metal nanoparticles has been used to generate steam for off-grid water purification and to sterilize medical instruments.[13,14,18−20] It has been shown that colloidal metal nanoparticles under irradiation can locally superheat water to temperatures greater than 300 °C without boiling due to the large Young−Laplace interfacial pressures that suppress bubble nucleation on highly curved nanoscale surfaces.[21−23] This important thermodynamic effect—where the Young−Laplace interfacial pressure, ΔP, is defined by the interfacial energy, γ, times the harmonic sum of the principle axes of curvature $(1/r_1 + 1/r_2)$ of the interface (*e.g.*, $\Delta P = 2\gamma/r$ for a sphere)—can lead to a much wider range of accessible temperatures to drive liquid-phase chemistry at nanoscale interfaces. While conventional liquid reactor systems are typically heated *via* thermal conduction across the interface between the reactor sidewall and the fluid, when the heat source is decoupled from the reactor sidewalls, bubble nucleation can be avoided, thereby increasing the accessible temperature range at standard pressures. Taking advantage of the nanoscale Young−Laplace effect, the irradiation of metal nanocrystals has been used to induce high-temperature reaction conditions at nanocrystal surfaces in a low-cost manner, fabricate crystalline inorganic nanomaterials,[24−26] and weld heterojunctions between nanowires.[17]

Metal nanocrystals are also essential for the growth of anisotropic semiconductor nanowires,[27,28] which have great potential in optoelectronic,[29,30] sensing,[31,32] energy conversion,[33−35] and energy storage applications.[36−38] Typically, semiconductor nanowires are grown *via* thermal decomposition of a semiconductor precursor and subsequent diffusion of semiconductor atoms into a metal nanocrystal seed. Upon

Received: January 25, 2021
Accepted: April 26, 2021

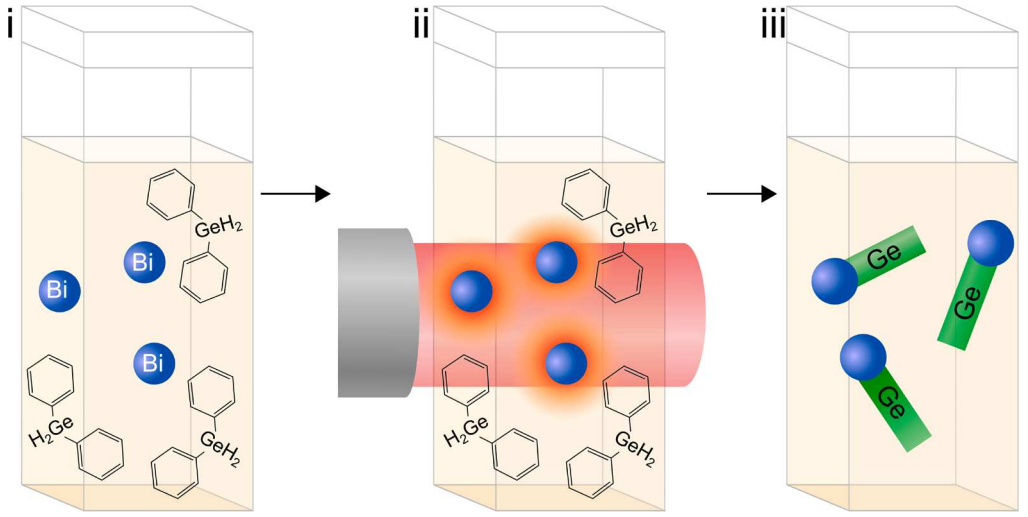

Figure 1. Illustration of contact-free, laser-driven, colloidal semiconductor nanowire growth in a high boiling point organic solvent on the benchtop in a quartz cuvette. (i–iii) The irradiation of colloidal metal nanocrystals with a collimated laser enables accumulation of thermal energy in solution, which can then be used to drive chemistry—such as the decomposition of molecular precursors—thus facilitating the contact-free, solution-based, photothermal synthesis of semiconductor nanowires.

saturation, the alloyed semiconductor-metal seeds facilitate nucleation and growth of crystalline semiconductor nanowires.[27] Although nanowire syntheses typically involve globally heating the reactor, some reports have used metal nanocrystals as both seeds for semiconductor nanowire growth and local heat sources under irradiation to drive precursor decomposition and diffusion.[10−12] For example, irradiating metal nanoparticle-decorated substrates in a modified chemical vapor deposition chamber enabled site-specific heating and, ultimately, plasmon-assisted growth of nanowire arrays[10] as well as single nanowires.[11,12] The irradiation of substrates decorated with metal nanoparticles submerged in solution has also been used to synthesize certain types of nanowires.[39−41] However, the growth of semiconductor nanowires dispersed in solution through laser irradiation of colloidal metal nanocrystals, which advantageously exploits the nanoscale Young–Laplace effect, remains largely unexplored.

In this work, we capitalize on the ability of colloidal metal nanoparticles to both photothermally heat under irradiation and to act as growth-directing seeds for the synthesis of semiconductor nanowires through a one-step, colloidal process. Rather than relying on global heating of the entire reactor system as in conventional colloidal syntheses, this approach transduces light into heat directly at the site of nanowire growth, thereby relaxing reactor design constraints to enable benchtop growth of semiconductor nanowires without the need for specialized, high-temperature, or high-pressure equipment. Through a combination of infrared thermal imaging and heat transfer models, we confirm that colloidal metal nanocrystals irradiated with a collimated near-infrared laser can reach the high temperatures (>200 °C) required for solution-phase nanowire synthesis due to a combination of the Young–Laplace effect and the collective heating effects of colloidal metallic nanoparticles and show the versatility of the process by growing three different example nanowire systems. This demonstrates a generalizable process for semiconductor nanowire growth that can be performed on a benchtop in either batch or continuous operation, for potential rapid, high-throughput screening and parameter optimization of semiconductor nanowire growth.

RESULTS AND DISCUSSION

This contact-free, laser-driven, solution-based nanowire growth process is detailed in Figure 1, which depicts a cuvette containing a dispersion of metal nanocrystals and molecular precursors (Figure 1i) in an organic solvent. Upon irradiation (Figure 1ii), the nanocrystals transduce the incident photons into thermal energy, which drives the decomposition of molecular semiconductor precursors, thereby inducing the formation of a saturated metal-semiconductor alloy that enables seeded nanowire growth (Figure 1iii).

While numerous studies have examined the heating of metal nanocrystals under irradiation, most investigations have focused on noble metals, such as gold.[13−16,21,22,42] To examine the potential heating effects enabled by contact-free irradiation of the low-melting point colloidal metal nanocrystals used in this study (Figure S1, Supporting Information (SI)), we irradiated bismuth nanocrystals in a 1 cm path length cuvette at a range of concentrations (Figure 2; Figure S2, Supporting Information), denoted by the optical density (defined as the ratio between the transmitted and incident irradiation intensity) of the bismuth nanocrystal dispersion at the excitation wavelength, λ = 1070 nm (abbreviated as OD_{1070}). Thermographic infrared images of a bismuth nanocrystal dispersion (OD_{1070} = 0.52) in octadecene in a cuvette under irradiation (Figure 2a–d; Movie S1, Supporting Information) demonstrate the photothermal transduction characteristics of the colloidal nanocrystals, as compared to neat solvent under identical excitation conditions (Figure 2e–h; Movie S1, Supporting Information). As the optical density of the Bi nanocrystal dispersion increases, the maximum temperature achieved increases to 191 °C (Figure 2i; Figure S2, Supporting Information), while the maximum cuvette temperature increases by only 17 °C over the same time period with only neat solvent present. Therefore, the observed temperature increase of the nanocrystal dispersions is due to photothermal transduction by the bismuth nanocrystals. We note that the thermographic images only reflect the temperature of the cuvette surface because the walls of the quartz cuvette absorb the long-wavelength infrared light used in thermographic imaging. Thus, the reaction volume is at a higher temperature

https://doi.org/10.1021/acsnano.1c00683
ACS Nano XXXX, XXX, XXX–XXX

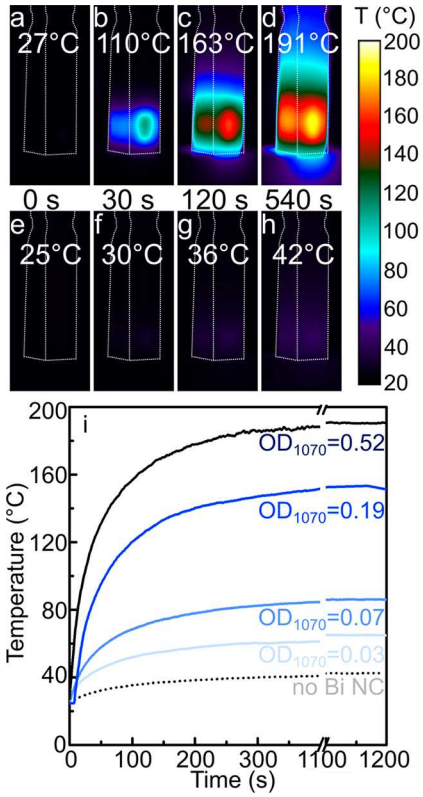

Figure 2. Time-dependent temperature of bismuth nanocrystal dispersions under continuous, near-infrared irradiation. (a–d) Thermographic infrared images illustrating the evolution of temperature during irradiation of a bismuth nanocrystal dispersion (OD_{1070} = 0.52) in a quartz cuvette with a near-infrared laser (1070 nm, 15 W), along with (e–h) a corresponding set of control images recorded for neat octadecene under identical irradiation conditions (1070 nm, 15 W) in the absence of nanocrystals (Movie S1, Supporting Information). Temperature labels correspond to the maximum temperature recorded in each image. (i) Time-dependent temperature profiles for a series of bismuth nanocrystal concentrations (OD_{1070} = 0.03–0.52) under 1070 nm irradiation (15 W).

due to the heat transfer resistance of both the solvent volume and the quartz cuvette walls (*vide infra*).

In addition to measuring the time dependence of the temperature profile on the bismuth nanocrystal concentration, we used COMSOL Multiphysics software to simulate the surface temperature of an irradiated cuvette containing a bismuth nanocrystal dispersion (Figure S3, Supporting Information). These numerical solutions accurately predict the surface temperature of the cuvette at low bismuth nanocrystal concentrations; however, the predicted temperatures diverge from the experimentally measured values at higher nanocrystal concentrations and higher irradiances. The divergent numerical solutions at higher bismuth nanocrystal concentrations are likely due to high-temperature effects, such as solvent convection and reflux, Ostwald ripening, or coalescence of bismuth nanocrystals, which are not included in the model. With these caveats, the numerical model provides an upper bound for the internal temperature profiles and demonstrates that the nanocrystals in the center of the cuvette reach high temperatures under laser irradiation (Figure S3, Supporting Information). Using an analytical solution based on a Mie theory source term,[43] we also calculated the temperatures of a single bismuth or indium nanocrystal (discussed later) suspended in an infinite bath of the growth solution. In this formalism, isolated bismuth and indium nanocrystals heat very little relative (ΔT < 1 K) to their surrounding solution volume and cannot decompose molecular precursors to drive nanowire growth (Figure S9, Supporting Information). The discrepancy between single-particle calculations and measured temperatures suggests that the nanocrystals heat *via* the collective scattering and absorption of photons. This is in agreement with previous work performed with gold nanoparticles in an aqueous solution under irradiation.[7,14,18,44] Baffou *et al.* identified a dimensionless number, ξ, to describe when collective heating effects become prominent in arrays of metal nanocrystals: $\xi = p^2/3RD$, where p is the mean first neighbor interdistance, R is the radius of the nanoparticle, and D is the characteristic illumination size.[44] Under these conditions, ξ is on the order of 10^{-3}, indicating that collective heating effects dominate. As a result, reaching the threshold temperature for nanowire growth depends on many factors, including the nanocrystal concentration, the thermal properties of the dispersion, and the irradiance of the incident laser.

Combined, these calculations and experimental results demonstrate that, while irradiated nanocrystals are responsible for heating the solution, temperature gradients between an individual nanocrystal and the surrounding solution are minimal. However, large temperature gradients do exist as a consequence of the gradients in irradiance that are present in the system (*i.e.*, between irradiated and nonirradiated portions of the solution) and gradients arising from the low thermal conductivity solvent (*i.e.*, between the center and edge of the irradiated region). These effects produce gradients in temperature at length scales on the order of ~0.1 mm, but not at the nanometer scale. As a lower bound, the finite-element model predicts that nanocrystals in the center of the cuvette are at least 10% (Kelvin scale) higher in temperature than the maximum surface temperature of the cuvette. For example, our simulations show that a cuvette with a surface temperature of 630 K (363 °C) has a temperature of ~700 K (430 °C) in the center of the reaction volume.

We next incorporated II–VI molecular precursors into the colloidal nanocrystal solution in an attempt to drive solution-liquid-solid (SLS) nanowire growth *via* photothermal heating. In a typical laser-driven synthesis, a solution of colloidal nanocrystals and molecular precursors in a cuvette was irradiated with a collimated laser. The optical density of the dispersion was observed to increase dramatically within the first 30 s of irradiation. When the laser was blocked, the reaction product rapidly flocculated, indicating a substantial change in morphology relative to the starting nanocrystals. Bright-field transmission electron microscopy (TEM) imaging (Figure 3b–d) clearly demonstrates that laser heating did not result in homogeneously nucleated CdSe byproducts upon precursor decomposition. Rather, the bismuth nanocrystal seeds act as growth-directing agents to produce CdSe nanowires *via* a photothermally driven SLS growth mechanism. Compared to previous two-step, optically driven II–IV nanowire growth processes,[41] the CdSe nanowire synthesis performed here was carried out in a single step. TEM images (Figure 3b–d) highlight the narrow nanowire diameters (7.3 ± 1.9 nm, Figure S5, Supporting Information) achieved *via* this photothermally driven process. High-resolution TEM (HR-TEM) imaging (Figure 3d) shows that the CdSe nanowires

https://doi.org/10.1021/acsnano.1c00683
ACS Nano XXXX, XXX, XXX–XXX

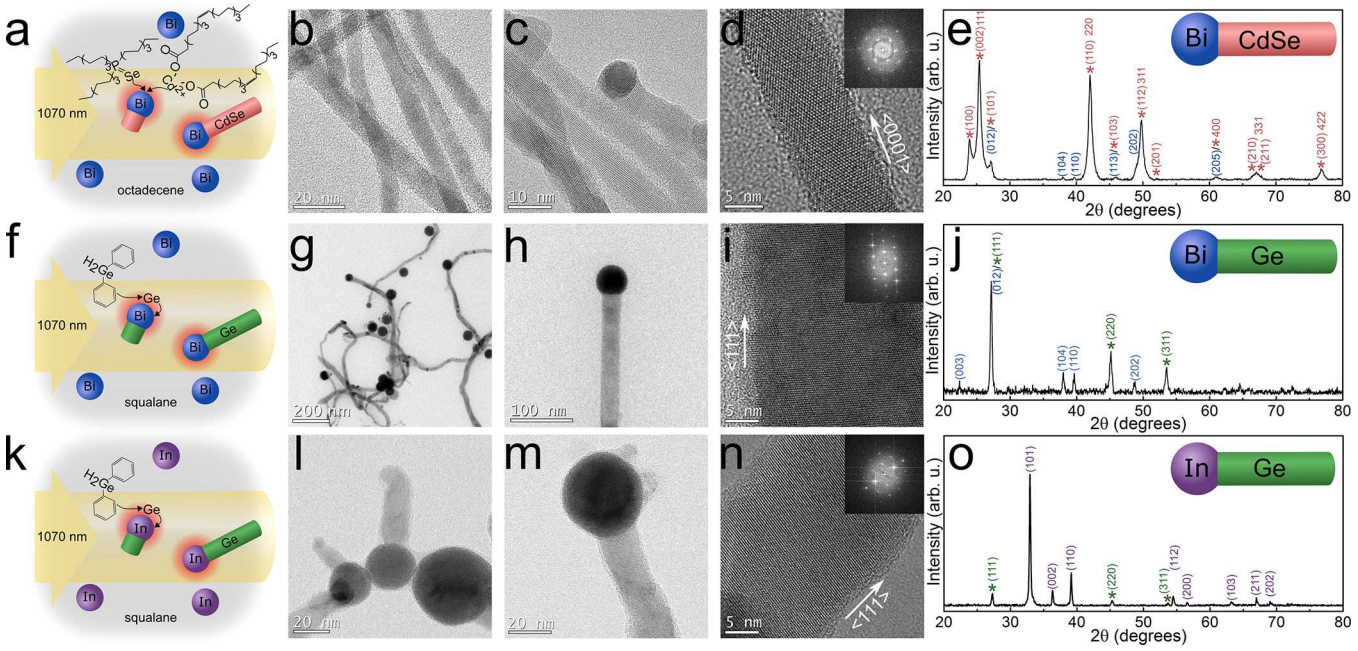

Figure 3. Examples of contact-free, solution-based, laser-driven nanowire growth on the benchtop for nanowire systems with both ionic and covalent character, produced using different metal nanocrystal seeds under 1070 nm excitation. (a–e) Narrow-diameter, polytypic wurtzite/zinc-blende CdSe nanowires (hexagonal reflection indices denoted in parentheses) grown from Bi nanocrystal seeds using cadmium oleate and trioctylphosphine selenide precursors. (f–j) Diamond-cubic, Bi-seeded Ge nanowires produced *via* photothermal decomposition of diphenylgermane. (k–o) In-seeded Ge nanowires grown using In nanocrystal seeds as photothermal heat sources. Both nanowire (highlighted with asterisks) and nanocrystal seed materials are indexed in each X-ray diffractogram.

exhibit the ⟨0001⟩ growth direction that is typical of anisotropic wurtzite-phase CdSe. X-ray diffraction (XRD) indicates that the CdSe nanowires are a mixture of wurtzite and zinc-blende phases, as is commonly observed in most CdSe nanowire syntheses; the mixture of the two phases can be attributed to the minimal energy difference between ⟨111⟩ zinc-blende and ⟨0001⟩ wurtzite nanowire growth.[45] Notably, XRD also shows an increased intensity of the (002) and (111) reflections for wurtzite and zinc-blende, respectively, which is consistent with previously reported CdSe nanowire growth directions associated with each phase (Figure 3e).[45] HR-TEM also indicates stacking faults along the length of the CdSe nanowire. Despite the temperature gradients, convection, and precursor diffusion that occurs during irradiation of the cuvette, analysis of the nanowire product indicates that the diameter distributions, morphologies, and growth directions of nanowires produced by photothermal heating are quite similar to those produced by conventional solution-liquid-solid (SLS)-based growth methods (see SI for further detailed discussion).[45] We also note that, under the irradiances investigated here, nanocrystal concentrations as low as OD_{1070} = 0.07 were still sufficient to photothermally synthesize semiconductor nanowires. The nanoparticle concentration could likely be further decreased by utilizing a focused beam,[17] increasing the irradiance, and optimizing the photothermal transduction characteristics of the excitation-source/nanocrystal pair. Control experiments based on the irradiation of CdSe molecular precursor solutions in the absence of bismuth nanocrystals resulted in minor temperature increases (Figure S2, Supporting Information) and no detectible precursor decomposition or nanowire growth. These results clearly demonstrate that, under irradiation, the bismuth nanocrystal dispersion heats rapidly, facilitating decomposition of the cadmium and selenium molecular precursors and subsequent solution-based growth of bismuth-seeded CdSe nanowires.

Notably, typical nanocrystal-seeded, SLS-based CdSe nanowire growth processes require the use of a Schlenk line and reaction temperatures in the range of 230–350 °C. Here, heat transduced by the nanocrystals in the contact-free, photothermal growth reaction enabled the same high temperature process to be carried out in a standard quartz cuvette on a benchtop. This is emphasized by the observation that the OD_{1070} = 0.07 Bi nanocrystal dispersion resulted in the successful growth of CdSe nanowires, despite the fact that the surface of the cuvette only reached a maximum temperature of 136 °C (Figure S2, Supporting Information). This result further indicates that the temperature at the nanocrystal-solvent interface is higher than the measured surface temperature of the cuvette. In addition to using a quartz cuvette as a reaction vessel, we have also successfully employed a simple nuclear magnetic resonance (NMR) tube combined with a low-cost, low-power (2 W), 808 nm diode to grow Bi-seeded CdSe nanowires (Movie S2, Supporting Information), demonstrating that optically driven nanowire growth can be carried out using a variety of excitation powers and wavelengths.

While this represents a successful demonstration of solution-based, photothermally driven seeded nanowire growth, CdSe has a large degree of ionic character, and material systems that are more covalent (such as Si and Ge) typically have much higher crystallization barriers and, therefore, require significantly higher temperatures (>300 °C) for nanowire growth.[46–49] To investigate the versatility of the photothermally driven nanowire growth process, we also targeted the production of group-IV semiconductor nanowires, using the same bismuth nanocrystal seeds to drive the reaction. In this scenario, colloidal bismuth nanocrystals under near-infrared

https://doi.org/10.1021/acsnano.1c00683
ACS Nano XXXX, XXX, XXX–XXX

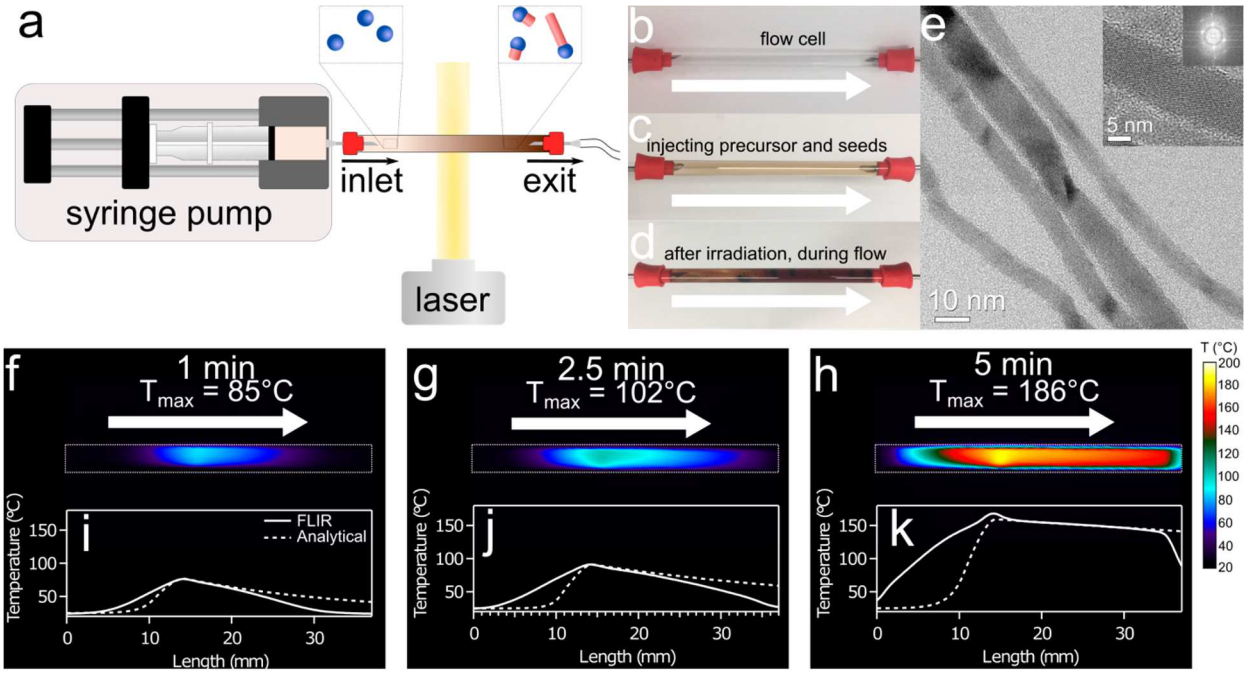

Figure 4. Demonstration of continuous, laser-driven nanowire growth under flow. (a) Flow cell schematic along with (b–d) associated images of the reaction zone (b) containing only octadecene, (c) during injection of Bi nanocrystal seeds (OD_{1070} = 0.07) and II–VI molecular precursors, and (d) after irradiation under flow. (e) Characteristic TEM images of the Bi-seeded CdSe nanowire product. (f–h) Snapshots from an infrared thermal imaging camera, showing spatial and temporal evolution of temperature profiles of the flow cell after 1, 2.5, and 5 min of 1070 nm irradiation under continuous flow (0.05 mL/min). Temperature labels correspond to the maximum temperature recorded in each image. (i–k) A comparison of the radially averaged FLIR temperatures (solid line) and analytically predicted temperatures (dashed line) of the flow cell after 1, 2.5, and 5 min of photothermal heating.

irradiation once again act both as heat sources and as seeds for nanowire growth, driving the decomposition of the diphenylgermane precursor to facilitate the optically driven SLS growth of Ge nanowires (Figure 3f–j) without the need for a vacuum system, Schlenk line, or supercritical reactor system. Bright-field TEM images (Figure 3g–i) demonstrate the growth of crystalline Ge nanowires with diameters of 15.6 ± 7.8 nm (Figure S6, Supporting Information) and a ⟨111⟩ growth direction, which is characteristic of high-temperature growth of Ge nanowires.[50] While the XRD diffractogram (Figure 3j) clearly shows the presence of both crystalline Bi and Ge, the Bi-seeded Ge nanowires synthesized through contact-free photothermal heating were typically observed to have a tortuous morphology, likely due to the small volume of solution that was irradiated, and subsequent convection of nanowires into and out of the beam.

To demonstrate the generality of this approach, we next investigated whether indium nanocrystals could be used for laser-driven nanowire growth. While indium has been used to grow germanium nanowires *via* vapor-liquid-solid growth[51] and other types of semiconductor nanowires through modified SLS growth,[48] previous work has primarily employed the use of evaporated In thin films to seed growth. Here, we demonstrate the use of colloidal In nanocrystals (Figure S7, Supporting Information) as photothermal heat transducers under incident near-infrared irradiation to decompose diphenylgermane in solution, once again enabling the laser-driven, seeded growth of germanium nanowires in a cuvette (Figure 3k–o). The In-seeded Ge nanowires generated from this optically driven process typically had shorter lengths and wider diameters (Figure 3k–o; Figure S8, Supporting Information) than the photothermally grown Bi-seeded Ge nanowires. These morphological differences can likely be attributed to the markedly lower melting point of In (156 °C) relative to Bi (271 °C), which could result in rapid coalescence of In nanoparticles upon heating, leading to larger seed particles and, thus, larger nanowire diameters. The differences in surface energies and contact angles for the two different nanocrystal seeds could also contribute to differences in morphology.

All of these processes generated SLS-grown nanowires under ambient conditions *via* photothermal heating without the use of a Schlenk line, pressure vessel, insulation, or resistive heating. Specifically, the high temperatures generated by contact-free, optical heating of the metal nanocrystals rapidly drive nanowire growth without the use of any high-temperature equipment. In comparison, global resistive heating during a conventional SLS nanowire growth reaction involves an isothermal process in which the reaction vessel and chemical components are at thermal equilibrium.

The versatility of this growth strategy naturally lends itself toward the integration of spectroscopic methods that could be used to study *in situ* nanowire growth dynamics and to rapidly tune reaction conditions. However, in all of the above nanowire growth demonstrations—using both quartz cuvettes and NMR tubes as reaction vessels—the nanowire growth solution inevitably developed convection currents due to the volume of the photothermal heating zone and variations in intensity across the Gaussian laser source relative to the solution volume. To realize the potential of this contact-free, colloidal nanocrystal-based semiconductor nanowire growth process, as a proof of principle, we demonstrated the photothermally driven growth of semiconductor nanowires using a continuous-flow reactor to circumvent problems associated with free convection and to validate laser-driven

https://doi.org/10.1021/acsnano.1c00683
ACS Nano XXXX, XXX, XXX–XXX

nanowire growth for future rapid screening of synthesis parameters (Figure 4). We first constructed an optically accessible reaction zone (Figure 4a), through which solutions of II−VI semiconductor precursors and colloidal nanocrystals could be injected simultaneously. Upon irradiation and while under flow, the nanocrystals once again rapidly generated heat to decompose the precursors and seed nanowire growth (Figure 4d,e), eventually exiting the flow cell further downstream. Converting this noncontact, laser-driven nanowire growth method into a continuous flow process is a further step toward an easily accessible, low-cost, scalable system in which nanowire growth dynamics and various growth parameters can be rapidly scanned and spectroscopically probed to enable real-time feedback and optimization of material properties.

To determine the internal temperature of the flow cell during heating, we analytically calculated the temperature profile within the reactor volume during laser-driven nanowire growth under flow.[52] We include details of the derivation and model, which should be valid for a wide range of flow rates, in the Supporting Information.[53] Briefly, we start from the energy equation

$$2\rho_s C_s v_z \frac{\partial T}{\partial z} = k_s\left[\frac{1}{r}\frac{\partial}{\partial r}\left(r\frac{\partial T}{\partial r}\right) + \frac{\partial^2 T}{\partial z^2}\right] + S \quad (1)$$

where ρ_s, C_s, and v_z are the density, heat capacity, and velocity of the solution in the flow reactor; T, z, and r are the temperature and axial and radial coordinates; and S is the source term. We solve the equation for three different regions: upstream of the irradiated region ($S = 0$), the region under laser irradiation ($S > 0$), and downstream of the laser irradiation ($S = 0$). At axial interfaces between these three regions, we match the temperatures and flux; at axial interfaces with inflow and outflow, we ensure the temperature is bounded as $z \rightarrow \pm\infty$; and for radial interfaces, we use a Robin's boundary condition based on correlations for natural conduction from a horizontal cylinder.[54]

At low flow rates, that is, for small Peclet numbers ($Pe < 10$), heat transport *via* both thermal conduction and thermal convection is important and cannot be neglected. The Peclet number is defined by $Pe = R_1\langle v_z\rangle/\alpha_s$ in which R_1 is the inner radius of the tube, and α_s is the thermal diffusivity of the fluid ($\alpha_s = k_s/\rho_s C_s$). Thermal camera images (Figure 4f−h) of the flow reactor clearly demonstrate axial diffusion of heat both upstream and downstream of the incident laser spot, experimentally verifying that axial conduction is taking place. Figure 4 (panels i−k) shows the projected temperature distribution on the surface of the flow cell and the analytically calculated, radially averaged temperature. The analysis reveals that there is a ∼1% gradient between the center of the reactor fluid volume and the surface of the chamber. This lack of a radial thermal gradient suggests that the maximum temperature during growth in the flow cell was ∼188 °C based on thermal camera images, which is less than the typical 230 °C temperature used in bismuth-seeded CdSe nanowire synthesis.[55] We note that analytical temperature distributions of both a bismuth-seeded CdSe nanowire and a bismuth nanocrystal (Figures S9 and S10, Supporting Information) in an infinite bath do not demonstrate appreciable heating above ambient temperatures.[17] It is possible that hot-electron effects or exothermic precursor decomposition may contribute to the energy required for semiconductor nanowire growth. To examine these possibilities, we photothermally heated colloidal bismuth nanocrystals in a cuvette and measured the surface temperatures with and without CdSe precursors (Figures S2 and S4, Supporting Information). After 9 min, the surfaces of the cuvettes containing the irradiated nanocrystal dispersions with CdSe precursors present were 96 °C higher in temperature than cuvettes without semiconductor precursors. This additional heating may be associated with an exothermic reaction of CdSe precursors, which may accelerate nanowire synthesis. Alternatively, the growth of nanowires may generate additional photon scattering or absorption effects that could boost the absorption of light, thus generating more heat. Supporting the above hypotheses, the analytically calculated temperature distributions for the flow reactor best match the measured temperature when the absorption efficiency and solution thermal conductivity increase over time, which would occur if either the growth of nanowires increases the absorption coefficient of the solution[56,57]—simultaneously increasing the thermal conductivity—and/or if the reaction is exothermic (Table S1, Supporting Information).

CONCLUSIONS

We have demonstrated that photothermal heating of colloidal metal nanocrystals *via* laser irradiation is a versatile approach to drive the solution-based synthesis of semiconductor nanowires with both ionic and covalent character. In these syntheses, Bi and In metal nanocrystals were used as contact-free photothermal transducers that facilitate the rapid SLS growth of semiconductor nanowires. Because these nanocrystals are dispersed in solution, rather than pinned to a substrate, they have the potential to locally superheat the solvent due to the large Young−Laplace interfacial surface pressure required to nucleate a bubble. Consequently, both temperature and gas handling constraints of the reactor are relaxed, enabling the use of low-cost quartz cuvettes or NMR tubes as benchtop reactors for nanowire synthesis. These results enable the translation from a batch process to a scalable, continuous-flow process. With further optimization, this optically driven synthesis could enable the solution-based growth of nanowires that currently cannot be synthesized in solution due to solvent boiling point limitations. In addition, photothermal heating makes rapid changes in temperature possible, which could facilitate the production of complex, heterostructured nanowires or rational dopant incorporation *via* solution-based methods. The ability to quickly reach high temperatures near the metal nanocrystal seed could potentially enable the nonequilibrium incorporation of atomically precise semiconductor dopants during the nanowire growth process, rather than during an additional postsynthetic doping step. Moreover, because this process can be performed on a benchtop in virtually any chemically inert, optically accessible reaction vessel, it could enable the direct integration of *in situ* scattering and spectroscopic techniques to study solution-based nanowire growth dynamics, rapid combinatorial scanning of nanowire chemistries, and optimize nanowire growth conditions with real-time feedback. This laser-driven nanowire growth strategy may also enable the study of single-particle nanowire growth dynamics through scattering measurements or the combination of *in situ* optical spectroscopy with single-beam laser tweezers.[17]

METHODS

Materials. All chemicals were used as received unless otherwise noted. Bismuth(III) chloride ($BiCl_3$, 99.99% trace metals basis),

https://doi.org/10.1021/acsnano.1c00683
ACS Nano XXXX, XXX, XXX−XXX

cadmium oxide (CdO, ≥99.9% trace metals basis), ethanol (anhydrous, ≤0.005% water), indium(III) chloride (99.999% trace metals basis), isopropanol (anhydrous, 99.5%), molecular sieves (3 Å), *n*-butyllithium (1.3 M in *n*-heptane), 1-octadecene (ODE, 90%), oleylamine (90%), oleic acid (degassed, 90%), sodium bis(trimethylsilyl)amide (1.0 M solution in tetrahydrofuran), squalane (96%), Super-Hydride solution (1.0 M lithium triethylborohydride in tetrahydrofuran), selenium (Se, <5 mm particle size, ≥99.999% trace metals basis), tetrahydrofuran (THF, anhydrous, ≥99.9%), toluene (anhydrous, 99.8%), and trioctylphosphine (TOP, 97%) were purchased from Sigma. Diphenylgermane (>95%) was purchased from Gelest. Poly(1-hexadecene-*co*-1-vinylpyrrolidinone) (PHD-*co*-PVP) was provided by Ashland under the trade name Ganex V-216. Toluene (Certified ACS, 99.8%) was purchased from Fisher. Ethanol (200 proof) was purchased from Decon Laboratories.

Bismuth Nanocrystal Synthesis. Bismuth nanocrystals were synthesized based on the protocol outlined by Wang *et al.*[55] A 25 wt % solution of PHD-*co*-PVP in 1-octadecene was dried over molecular sieves for 1 week. $BiCl_3$ (2.6×10^{-2} mmol) was mixed at 800 rpm with THF (570 μL) under nitrogen for 30 min. The solution of PHD-*co*-PVP in octadecene (6.1 mL) was added to the flask under continuous mixing at 900 rpm. The flask was cycled between nitrogen and vacuum three times. A solution of 1.0 M sodium bis(trimethylsilyl)amide in THF (825 μL) was injected, and the flask was stirred until a dark orange-brown color was observed (~10 min, 1100 rpm). The solution was then heated to 200 °C for 17 h, cooled, and then transferred into a nitrogen-filled glovebox for storage. Bismuth nanocrystals were handled under nitrogen for cleaning. Nanocrystals were washed five times using a 1:4 ratio of anhydrous hexanes:ethanol and centrifugation (6800 RCF for 10 min) to remove excess PHD-*co*-PVP prior to use for nanowire growth. The average diameter of the bismuth nanocrystal seeds was 52 ± 8 nm.

Indium Nanocrystal Synthesis. Indium nanocrystals were synthesized using the protocol outlined by He *et al.*[58] $InCl_3$ (1.4×10^{-1} mmol) was measured in the glovebox, transferred into a three-neck flask, and attached to a Schlenk line. The flask was purged with nitrogen and then transitioned between vacuum and nitrogen atmosphere three times. Oleylamine (13 mL) was added to the flask, which was heated to 100 °C while mixing (1000 rpm) and then placed under vacuum for an additional 45 min. The mixture was blanketed with nitrogen and further heated to 160 °C. A solution of 1.3 M *n*-butyllithium in *n*-heptane (1.3 mL) was injected into the flask, followed by an injection of 1.0 M Super-Hydride solution (300 μL). The reaction was allowed to run for 10 s, whereupon 12 mL of anhydrous toluene was injected to cool the solution and quench the reaction. At 50 °C, oleic acid (400 μL) was added to stabilize the nanocrystals. Nanocrystals were then transferred into a glovebox and handled under nitrogen for cleaning. Anhydrous ethanol (12 mL) was added to the dispersion, which was centrifuged at 4180 RCF for 10 min. The supernatant was discarded, and the nanocrystals were washed with a 2:1 ratio of anhydrous hexanes:ethanol three more times. The average diameter of the indium nanocrystal seeds was 16 ± 2 nm.

Cadmium Oleate. Using standard Schlenk line techniques, 0.15 M cadmium oleate in 1-octadecene (ODE) was prepared by combining 210 mg of CdO, 2.7 g of oleic acid, and 5.2 g of ODE in a flask. The mixture was blanketed with nitrogen and stirred at 800 rpm, heated to 110 °C, and placed under vacuum for 30 min. The mixture was cooled to room temperature under nitrogen and transferred to a glovebox, whereupon 1 mL of trioctylphosphine (TOP) was added and mixed for 15 min.

Trioctylphospine-Selenide (TOP:Se). A 1.0 M stock solution of TOP:Se was prepared in a nitrogen-filled glovebox by stirring 238 mg of Se in 5 mL of TOP overnight, until dissolved.

Nanowire Precursor Solutions for Photothermal Nanowire Growth. All nanowire precursor growth solutions were prepared and mixed under a nitrogen atmosphere in a quartz cuvette, which was lined with a thin layer of Teflon tape prior to sealing with a screw cap. The cap was then wrapped with Parafilm to avoid inadvertent nanocrystal oxidation.

Bi-Seeded Cadmium Selenide Nanowire Growth Solution. The Bi-seeded CdSe nanowire precursor growth solution was prepared under a nitrogen atmosphere in a quartz cuvette. 50 μL of a Bi nanocrystal dispersion (1.34 mg elemental Bi/L) in hexane, 125 μL of Cd-oleate (0.15 M in ODE), and 213 μL of TOP:Se (1.0 M in ODE) were combined and mixed in a screw-top quartz cuvette.

Bi-Seeded Germanium Nanowire Growth Solution. The Bi-seeded Ge nanowire precursor growth solution was prepared under a nitrogen atmosphere in a quartz cuvette. 50 μL of a Bi nanocrystal dispersion (1.34 mg elemental Bi/L) in hexane, 100 μL of diphenylgermane (DPG), and 150 μL of squalane were combined and mixed in a screw-top quartz cuvette.

In-Seeded Germanium Nanowire Growth Solution. The In-seeded Ge nanowire precursor growth solution was prepared under a nitrogen atmosphere in a quartz cuvette. 50 μL of an In nanocrystal dispersion in hexane, 100 μL of diphenylgermane (DPG), and 150 μL of squalane were combined and mixed in a screw-top quartz cuvette.

Laser-Driven Nanowire Growth. Nanowire precursor growth solutions consisting of metal nanocrystals, molecular semiconductor precursors, and degassed solvents (squalane or ODE) were loaded into a screw-top quartz cuvette in the glovebox, where the top of the cuvette was lined with Teflon and then wrapped with Parafilm to prevent oxidation of nanocrystals. The cuvette with the growth solution was transferred out of the glovebox and subsequently irradiated with an unpolarized, Gaussian, near-infrared fiber laser (λ = 1070 nm) with a spot size of 5 mm at a range of powers (15−70 W) and times (5−20 min). The resulting product was washed with a 2:1 ratio of toluene and ethanol, collected by centrifugation at 19 000 RCF, dispersed in toluene, and washed two more times.

Continuous-Flow Photothermal Nanowire Growth. For a typical continuous flow-based, photothermally driven nanowire growth synthesis, a glass tube with an inner diameter, outer diameter, and length of 4, 5, and 95 mm, respectively, was sealed under a nitrogen atmosphere with two small rubber septa. The reaction vessel was prefilled with degassed 1-octadecene to displace all nitrogen prior to injection of the nanowire growth solution. The nanowire precursor growth solution, consisting of 60 μL of a Bi nanocrystal dispersion (1.34 mmol/L), 750 μL of Cd-oleate (0.15 M), 1.3 mL of TOP:Se (1.0 M), and 240 μL of degassed ODE, was prepared in a nitrogen-filled glovebox and loaded into a syringe. The needle of the precursor syringe was inserted through a rubber septum leading into the reaction vessel, and the syringe was fixed onto a syringe pump in order to control the flow rate (5 mL/h). A second needle was inserted into the other rubber septum on the exit side of the reaction vessel, leading to a glass vial used to collect the nanowire product. Prior to injecting the nanowire precursor growth solution, the laser was aligned to irradiate the center of the reaction vessel. After injecting the glass reactor vessel with the nanowire precursor solution, the reactor was irradiated with an unpolarized, Gaussian, near-infrared fiber laser (λ = 1070 nm) at 5 W. The product was washed with a 2:1:1 ratio of toluene:chloroform:ethanol, collected by centrifugation at 19 000 RCF, dispersed into toluene, and washed two more times prior to sample characterization.

Materials Characterization. TEM images were acquired with an FEI Tecnai G2 F20 Supertwin TEM operating with a 200 kV accelerating voltage and were analyzed using ImageJ Software. XRD scans were collected using a Bruker D8 Discover equipped with an IμS 2-D XRD detector system and were analyzed using EVA software. Inductively coupled plasma optical emission spectroscopy (ICP-OES) was performed with a PerkinElmer Optima 8300 spectrophotometer. UV−vis extinction spectra were collected using an Agilent Cary 60 UV−vis spectrophotometer. Time-dependent infrared thermal imaging was performed with an FLIR A325sc camera using the 0−350 °C temperature range setting, and the resulting videos were analyzed using ResearchIR software.

https://doi.org/10.1021/acsnano.1c00683
ACS Nano XXXX, XXX, XXX−XXX

ASSOCIATED CONTENT

Supporting Information

The Supporting Information is available free of charge at https://pubs.acs.org/doi/10.1021/acsnano.1c00683.

Characterization of nanocrystals; characterization of nanowire diameters; analytical heat transport models of nanocrystals and nanowires; finite-element heat transport solutions; and the analytical heat transport derivation of the continuous flow reactor (PDF)

Movie showing thermographic imaging of the evolution of temperature of a cuvette containing a bismuth nanocrystal dispersion under irradiation (MP4)

Movie showing the growth of Bi-seeded CdSe in an NMR tube using laser irradiation (MP4)

AUTHOR INFORMATION

Corresponding Authors

Peter J. Pauzauskie − *Department of Chemical Engineering, University of Washington, Seattle, Washington 98195-1750, United States; Department of Materials Science and Engineering, University of Washington, Seattle, Washington 98195-2120, United States; Molecular Engineering & Sciences Institute, University of Washington, Seattle, Washington 98195-1652, United States; Physical and Computational Sciences Directorate, Pacific Northwest National Laboratory, Richland, Washington 99352, United States;* orcid.org/0000-0002-1554-5949; Email: peterpz@uw.edu

Vincent C. Holmberg − *Department of Chemical Engineering, University of Washington, Seattle, Washington 98195-1750, United States; Molecular Engineering & Sciences Institute, University of Washington, Seattle, Washington 98195-1652, United States; Clean Energy Institute, University of Washington, Seattle, Washington 98195-1653, United States;* orcid.org/0000-0002-9591-8951; Email: holmvc@uw.edu

Authors

Elena P. Pandres − *Department of Chemical Engineering, University of Washington, Seattle, Washington 98195-1750, United States;* orcid.org/0000-0003-1435-5614

Matthew J. Crane − *Department of Chemical Engineering, University of Washington, Seattle, Washington 98195-1750, United States;* orcid.org/0000-0001-8461-4808

E. James Davis − *Department of Chemical Engineering, University of Washington, Seattle, Washington 98195-1750, United States*

Complete contact information is available at: https://pubs.acs.org/10.1021/acsnano.1c00683

Author Contributions

#These authors contributed equally to this work. E.P.P. and M.J.C. performed the experiments and contributed equally to this work. M.J.C., P.J.P., and E.J.D. performed the heat transport analysis. M.J.C., E.P.P., V.C.H., and P.J.P. conceived the experiments. V.C.H. and P.J.P. directed the research. All authors contributed to the design of experiments, scientific discussion, and writing of the manuscript.

Notes

This manuscript has been previously submitted to a preprint server: Pandres, E. P.; Crane, M. J.; Davis, E. J.; Pauzauskie, P. J.; Holmberg, V.C. Laser-Driven Growth of Semiconductor Nanowires from Colloidal Nanocrystals *via* the Young−Laplace Effect. *arXiv.org*. 2020, 2007.09305. https://arxiv.org/abs/2007.09305 (accessed 2020-07-18).

The authors declare no competing financial interest.

ACKNOWLEDGMENTS

The authors thank Soohyung Lee for assistance with ICP-OES measurements. This research was supported by the National Science Foundation (NSF) through the UW Molecular Engineering Materials Center, a Materials Research Science and Engineering Center (DMR-1719797), the University of Washington Molecular Engineering Institute, and the State of Washington through the University of Washington Clean Energy Institute and *via* funding from the Washington Research Foundation. Part of this work was conducted at the Molecular Analysis Facility, a National Nanotechnology Coordinated Infrastructure site at the University of Washington which is supported in part by the National Science Foundation (grant ECC-1542101), the University of Washington, the Molecular Engineering & Sciences Institute, and the Clean Energy Institute. M.J.C. acknowledges a NDSEG Fellowship as well as a WRF Postdoctoral Fellowship. P.J.P. acknowledges support from UW's Institute for Nanoengineered Systems (NanoES).

REFERENCES

(1) Kloxin, A. M.; Kasko, A. M.; Salinas, C. N.; Anseth, K. S. Photodegradable Hydrogels for Dynamic Tuning of Physical and Chemical Properties. *Science* **2009**, *324*, 59−63.

(2) Badeau, B. A.; Comerford, M. P.; Arakawa, C. K.; Shadish, J. A.; DeForest, C. A. Engineered Modular Biomaterial Logic Gates for Environmentally Triggered Therapeutic Delivery. *Nat. Chem.* **2018**, *10*, 251−258.

(3) Buriak, J. M. Illuminating Silicon Surface Hydrosilylation: An Unexpected Plurality of Mechanisms. *Chem. Mater.* **2014**, *26*, 763−772.

(4) Kelly, J. A.; Veinot, J. G. C. An Investigation into Near-UV Hydrosilylation of Freestanding Silicon Nanocrystals. *ACS Nano* **2010**, *4*, 4645−4656.

(5) Mukherjee, S.; Zhou, L.; Goodman, A. M.; Large, N.; Ayala-Orozco, C.; Zhang, Y.; Nordlander, P.; Halas, N. J. Hot-Electron-Induced Dissociation of H_2 on Gold Nanoparticles Supported on SiO_2. *J. Am. Chem. Soc.* **2014**, *136*, 64−67.

(6) Enright, M. J.; Gilbert-Bass, K.; Sarsito, H.; Cossairt, B. M. Photolytic C−O Bond Cleavage with Quantum Dots. *Chem. Mater.* **2019**, *31*, 2677−2682.

(7) Robatjazi, H.; Zhao, H.; Swearer, D. F.; Hogan, N. J.; Zhou, L.; Alabastri, A.; McClain, M. J.; Nordlander, P.; Halas, N. J. Plasmon-Induced Selective Carbon Dioxide Conversion on Earth-Abundant Aluminum-Cuprous Oxide Antenna-Reactor Nanoparticles. *Nat. Commun.* **2017**, *8*, 27.

(8) Erickson, D.; Sinton, D.; Psaltis, D. Optofluidics for Energy Applications. *Nat. Photonics* **2011**, *5*, 583−590.

(9) Adleman, J. R.; Boyd, D. A.; Goodwin, D. G.; Psaltis, D. Heterogenous Catalysis Mediated by Plasmon Heating. *Nano Lett.* **2009**, *9*, 4417−4423.

(10) Boyd, D. A.; Greengard, L.; Brongersma, M.; El-Naggar, M. Y.; Goodwin, D. G. Plasmon-Assisted Chemical Vapor Deposition. *Nano Lett.* **2006**, *6*, 2592−2597.

(11) Cao, L.; Barsic, D. N.; Guichard, A. R.; Brongersma, M. L. Plasmon-Assisted Local Temperature Control to Pattern Individual Semiconductor Nanowires and Carbon Nanotubes. *Nano Lett.* **2007**, *7*, 3523−3527.

(12) Di Martino, G.; Michaelis, F. B.; Salmon, A. R.; Hofmann, S.; Baumberg, J. J. Controlling Nanowire Growth by Light. *Nano Lett.* **2015**, *15*, 7452−7457.

(13) Neumann, O.; Urban, A. S.; Day, J.; Lal, S.; Nordlander, P.; Halas, N. J. Solar Vapor Generation Enabled by Nanoparticles. *ACS Nano* **2013**, *7*, 42−49.
(14) Fang, Z.; Zhen, Y.-R.; Neumann, O.; Polman, A.; García de Abajo, F. J.; Nordlander, P.; Halas, N. J. Evolution of Light-Induced Vapor Generation at a Liquid-Immersed Metallic Nanoparticle. *Nano Lett.* **2013**, *13*, 1736−1742.
(15) Baral, S.; Green, A. J.; Livshits, M. Y.; Govorov, A. O.; Richardson, H. H. Comparison of Vapor Formation of Water at the Solid/Water Interface to Colloidal Solutions Using Optically Excited Gold Nanostructures. *ACS Nano* **2014**, *8*, 1439−1448.
(16) Richardson, H. H.; Hickman, Z. N.; Govorov, A. O.; Thomas, A. C.; Zhang, W.; Kordesch, M. E. Thermooptical Properties of Gold Nanoparticles Embedded in Ice: Characterization of Heat Generation and Melting. *Nano Lett.* **2006**, *6*, 783−788.
(17) Crane, M. J.; Pandres, E. P.; Davis, E. J.; Holmberg, V. C.; Pauzauskie, P. J. Optically Oriented Attachment of Nanoscale Metal-Semiconductor Heterostructures in Organic Solvents *via* Photonic Nanosoldering. *Nat. Commun.* **2019**, *10*, 4942.
(18) Hogan, N. J.; Urban, A. S.; Ayala-Orozco, C.; Pimpinelli, A.; Nordlander, P.; Halas, N. J. Nanoparticles Heat Through Light Localization. *Nano Lett.* **2014**, *14*, 4640−4645.
(19) Neumann, O.; Feronti, C.; Neumann, A. D.; Dong, A.; Schell, K.; Lu, B.; Kim, E.; Quinn, M.; Thompson, S.; Grady, N.; Nordlander, P.; Oden, M.; Halas, N. J. Compact Solar Autoclave Based on Steam Generation Using Broadband Light-Harvesting Nanoparticles. *Proc. Natl. Acad. Sci. U. S. A.* **2013**, *110*, 11677−11681.
(20) Dongare, P. D.; Alabastri, A.; Pedersen, S.; Zodrow, K. R.; Hogan, N. J.; Neumann, O.; Wu, J.; Wang, T.; Deshmukh, A.; Elimelech, M.; Li, Q.; Nordlander, P.; Halas, N. J. Nanophotonics-Enabled Solar Membrane Distillation for Off-Grid Water Purification. *Proc. Natl. Acad. Sci. U. S. A.* **2017**, *114*, 6936−6941.
(21) Kyrsting, A.; Bendix, P. M.; Stamou, D. G.; Oddershede, L. B. Heat Profiling of Three-Dimensionally Optically Trapped Gold Nanoparticles Using Vesicle Cargo Release. *Nano Lett.* **2011**, *11*, 888−892.
(22) Carlson, M. T.; Green, A. J.; Richardson, H. H. Superheating Water by CW Excitation of Gold Nanodots. *Nano Lett.* **2012**, *12*, 1534−1537.
(23) Baffou, G.; Polleux, J.; Rigneault, H.; Monneret, S. Super-Heating and Micro-Bubble Generation Around Plasmonic Nanoparticles under Cw Illumination. *J. Phys. Chem. C* **2014**, *118*, 4890−4898.
(24) Robert, H. M. L.; Kundrat, F.; Bermúdez-Ureña, E.; Rigneault, H.; Monneret, S.; Quidant, R.; Polleux, J.; Baffou, G. Light-Assisted Solvothermal Chemistry Using Plasmonic Nanoparticles. *ACS Omega* **2016**, *1*, 2−8.
(25) Christopher, P.; Xin, H.; Linic, S. Visible-Light-Enhanced Catalytic Oxidation Reactions on Plasmonic Silver Nanostructures. *Nat. Chem.* **2011**, *3*, 467−472.
(26) Qiu, J.; Wei, W. D. Surface Plasmon-Mediated Photothermal Chemistry. *J. Phys. Chem. C* **2014**, *118*, 20735−20749.
(27) Dasgupta, N. P.; Sun, J.; Liu, C.; Brittman, S.; Andrews, S. C.; Lim, J.; Gao, H.; Yan, R.; Yang, P. 25th Anniversary Article: Semiconductor Nanowires − Synthesis, Characterization, and Applications. *Adv. Mater.* **2014**, *26*, 2137−2184.
(28) Crane, M. J.; Pauzauskie, P. J. Mass Transport in Nanowire Synthesis: An Overview of Scalable Nanomanufacturing. *J. Mater. Sci. Technol.* **2015**, *31*, 523−532.
(29) Quan, L. N.; Kang, J.; Ning, C.-Z.; Yang, P. Nanowires for Photonics. *Chem. Rev.* **2019**, *119*, 9153−9169.
(30) Huang, J.; Lai, M.; Lin, J.; Yang, P. Rich Chemistry in Inorganic Halide Perovskite Nanostructures. *Adv. Mater.* **2018**, *30*, 1802856.
(31) Cui, Y.; Wei, Q.; Park, H.; Lieber, C. M. Nanowire Nanosensors for Highly Sensitive and Selective Detection of Biological and Chemical Species. *Science* **2001**, *293*, 1289−1292.
(32) Patolsky, F.; Lieber, C. M. Nanowire Nanosensors. *Mater. Today* **2005**, *8*, 20−28.
(33) Hochbaum, A. I.; Yang, P. Semiconductor Nanowires for Energy Conversion. *Chem. Rev.* **2010**, *110*, 527−546.
(34) Åberg, I.; Vescovi, G.; Asoli, D.; Naseem, U.; Gilboy, J. P.; Sundvall, C.; Dahlgren, A.; Svensson, K. E.; Anttu, N.; Björk, M. T.; Samuelson, L. A GaAs Nanowire Array Solar Cell with 15.3% Efficiency at 1 Sun. *IEEE J. Photovolt.* **2016**, *6*, 185−190.
(35) Su, Y.; Liu, C.; Brittman, S.; Tang, J.; Fu, A.; Kornienko, N.; Kong, Q.; Yang, P. Single-Nanowire Photoelectrochemistry. *Nat. Nanotechnol.* **2016**, *11*, 609−612.
(36) Chan, C. K.; Peng, H.; Liu, G.; McIlwrath, K.; Zhang, X. F.; Huggins, R. A.; Cui, Y. High-Performance Lithium Battery Anodes Using Silicon Nanowires. *Nat. Nanotechnol.* **2008**, *3*, 31−35.
(37) Chan, C. K.; Patel, R. N.; O'Connell, M. J.; Korgel, B. A.; Cui, Y. Solution-Grown Silicon Nanowires for Lithium-Ion Battery Anodes. *ACS Nano* **2010**, *4*, 1443−1450.
(38) Chockla, A. M.; Harris, J. T.; Akhavan, V. A.; Bogart, T. D.; Holmberg, V. C.; Steinhagen, C.; Mullins, C. B.; Stevenson, K. J.; Korgel, B. A. Silicon Nanowire Fabric as a Lithium Ion Battery Electrode Material. *J. Am. Chem. Soc.* **2011**, *133*, 20914−20921.
(39) Chen, X.; Liu, R.; Qiao, S.; Mao, J.; Du, X. Synthesis of Cadmium Chalcogenides Nanowires *via* Laser-Activated Gold Catalysts in Solution. *Mater. Chem. Phys.* **2018**, *212*, 408−414.
(40) Huang, C.; Mao, J.; Chen, X. M.; Yang, J.; Du, X. W. Laser-Activated Gold Catalysts for Liquid-Phase Growth of Cadmium Selenide Nanowires. *Chem. Commun.* **2015**, *51*, 2145−2148.
(41) Chen, X.-M.; Mao, J.; Zhou, Y.-Z.; Yang, J.; Du, X.-W.; Qiao, S.-Z. Laser-Driven Absorption/Desorption of Catalysts for Producing Nanowire Arrays in Solution. *J. Mater. Chem. A* **2016**, *4*, 379−383.
(42) Lukianova-Hleb, E.; Hu, Y.; Latterini, L.; Tarpani, L.; Lee, S.; Drezek, R. A.; Hafner, J. H.; Lapotko, D. O. Plasmonic Nanobubbles as Transient Vapor Nanobubbles Generated Around Plasmonic Nanoparticles. *ACS Nano* **2010**, *4*, 2109−2123.
(43) Crane, M. J.; Smith, B. E.; Meisenheimer, P. B.; Zhou, X.; Stroud, R. M.; James Davis, E.; Pauzauskie, P. J. Photothermal Effects During Nanodiamond Synthesis from a Carbon Aerogel in a Laser-Heated Diamond Anvil Cell. *Diamond Relat. Mater.* **2018**, *87*, 134−142.
(44) Baffou, G.; Berto, P.; Bermúdez Ureña, E.; Quidant, R.; Monneret, S.; Polleux, J.; Rigneault, H. Photoinduced Heating of Nanoparticle Arrays. *ACS Nano* **2013**, *7*, 6478−6488.
(45) Kuno, M. An Overview of Solution-Based Semiconductor Nanowires: Synthesis and Optical Studies. *Phys. Chem. Chem. Phys.* **2008**, *10*, 620−639.
(46) Hanrath, T.; Korgel, B. A. Supercritical Fluid−Liquid−Solid (SFLS) Synthesis of Si and Ge Nanowires Seeded by Colloidal Metal Nanocrystals. *Adv. Mater.* **2003**, *15*, 437−440.
(47) Trentler, T. J.; Hickman, K. M.; Goel, S. C.; Viano, A. M.; Gibbons, P. C.; Buhro, W. E. Solution-Liquid-Solid Growth of Crystalline III-V Semiconductors: An Analogy to Vapor-Liquid-Solid Growth. *Science* **1995**, *270*, 1791−1794.
(48) Geaney, H.; Kennedy, T.; Dickinson, C.; Mullane, E.; Singh, A.; Laffir, F.; Ryan, K. M. High Density Growth of Indium Seeded Silicon Nanowires in the Vapor Phase of a High Boiling Point Solvent. *Chem. Mater.* **2012**, *24*, 2204−2210.
(49) Chockla, A. M.; Harris, J. T.; Korgel, B. A. Colloidal Synthesis of Germanium Nanorods. *Chem. Mater.* **2011**, *23*, 1964−1970.
(50) Hanrath, T.; Korgel, B. A. Crystallography and Surface Faceting of Germanium Nanowires. *Small* **2005**, *1*, 717−721.
(51) Sun, X.; Calebotta, G.; Yu, B.; Selvaduray, G.; Meyyappan, M. Synthesis of Germanium Nanowires on Insulator Catalyzed by Indium or Antimony. *J. Vac. Sci. Technol. B Microelectron. Nanometer Struct. Process. Meas. Phenom.* **2007**, *25*, 415−420.
(52) Crane, M. J.; Zhou, X.; Davis, E. J.; Pauzauskie, P. J. Photothermal Heating and Cooling of Nanostructures. *Chem. - Asian J.* **2018**, *13*, 2575−2586.
(53) Davis, E. J. Exact Solutions for a Class of Heat and Mass Transfer Problems. *Can. J. Chem. Eng.* **1973**, *51*, 562−572.

https://doi.org/10.1021/acsnano.1c00683
ACS Nano XXXX, XXX, XXX−XXX

(54) Churchill, S. W.; Chu, H. H. S. Correlating Equations for Laminar and Turbulent Free Convection from a Horizontal Cylinder. *Int. J. Heat Mass Transfer* **1975**, *18*, 1049−1053.
(55) Wang, F.; Buhro, W. E. An Easy Shortcut Synthesis of Size-Controlled Bismuth Nanoparticles and Their Use in the SLS Growth of High-Quality Colloidal Cadmium Selenide Quantum Wires. *Small* **2010**, *6*, 573−581.
(56) Wang, S.; Cheng, Y.; Wang, R.; Sun, J.; Gao, L. Highly Thermal Conductive Copper Nanowire Composites with Ultralow Loading: Toward Applications as Thermal Interface Materials. *ACS Appl. Mater. Interfaces* **2014**, *6*, 6481−6486.
(57) Balachander, N.; Seshadri, I.; Mehta, R. J.; Schadler, L. S.; Borca-Tasciuc, T.; Keblinski, P.; Ramanath, G. Nanowire-Filled Polymer Composites with Ultrahigh Thermal Conductivity. *Appl. Phys. Lett.* **2013**, *102*, No. 093117.
(58) He, M.; Protesescu, L.; Caputo, R.; Krumeich, F.; Kovalenko, M. V. A General Synthesis Strategy for Monodisperse Metallic and Metalloid Nanoparticles (In, Ga, Bi, Sb, Zn, Cu, Sn, and Their Alloys) *via in Situ* Formed Metal Long-Chain Amides. *Chem. Mater.* **2015**, *27*, 635−647.

https://doi.org/10.1021/acsnano.1c00683
ACS Nano XXXX, XXX, XXX−XXX